J. Fluid Mech. (1984) *vol.* 146, *pp.* 203–225
Printed in Great Britain

Asymmetric flow between parallel rotating disks

By C.-Y. LAI, K. R. RAJAGOPAL AND A. Z. SZERI
Department of Mechanical Engineering, University of Pittsburgh, Pittsburgh, PA 15261

(Received 13 January 1984)

Flows occurring between parallel rotating disks have recently been generalized by Parter & Rajagopal (1984) to include solutions that are not axisymmetric. They prove existence, whereas in the present paper we report, for the first time, numerical results for two cases: (i) rotation about a common axis, and (ii) rotation about distinct axes. Calculations were performed for two values of the Ekman number $E = \nu/d^2\omega$ at the relative disk rotations of $s = 0.8$, $s = 0$ and $s = -0.25$, where $s = \omega_2/\omega_1$.

1. Introduction

Kármán's (1921) pioneering study of steady axisymmetric flow induced by a single rotating disk has been followed by intensive studies of flow due to a single disk and flow between two disks rotating about coincident axes. These studies cover a broad spectrum. They range from papers primarily concerned with the physics and/or the numerical modelling of the problem, to those in which formal and rigorous mathematical results are established. Numerical calculations have been carried out by Lance & Rogers (1961), Pearson (1965), Mellor, Chapple & Stokes (1968), Greenspan (1972), Nguyen, Ribault & Florent (1975), Roberts & Shipman (1976), Holodniok, Kubíček & Hlaváček (1977, 1981), Wilson & Schryer (1978), Adams & Szeri (1982), Keller & Szeto (1983), Dijkstra & van Heijst (1983) and Szeri *et al.* (1983*b*). Despite such a detailed study, basic questions regarding the 'existence' and 'uniqueness' of these solutions remain unanswered. A discussion of these topics can be found in a recent review article by Parter (1982).

All the above studies employ the classical Kármán assumption, viz. that the axial velocity is independent of radial position and that the flow is axisymmetric. Recently Berker (1979) considered the flow between corotating disks and established a one-parameter family of solutions. The only axisymmetric solution in this family is the rigid-body motion; thus it is just this solution that would follow from Kármán's assumptions. In the light of Berker's work, one is advised to reexamine the classical problem of flow between parallel rotating disks, within the context of establishing asymmetric solutions. This has been recently carried out by Parter & Rajagopal (1984), who prove the existence of a one-parameter family of solutions for flow between two disks rotating about a common axis, or about distinct axes. In the case of rotation of the disks about distinct axes, but with the same angular velocities, Abbot & Walters (1970) have exhibited an exact solution, Although they restricted themselves to midplane symmetry, it is clear that a one-parameter family, as proved by Berker (1979) is also possible in their problem as suggested by the analysis of Rajagopal & Gupta (1981). Berker's solutions and those of Abbot & Walters belong to the class of pseudoplane flows which have been studied earlier by Berker (1936). The flow between disks rotating about non-coincident axes with equal angular velocity has relevance to the flow that occurs in the orthogonal rheometer, an instrument used to characterize the material moduli of fluids. Such flows are special

in that they are motions with constant principal relative stretch history. They have been studied in considerable detail (Rajagopal 1981). Asymmetric solutions identical to Berker's in structure have also been obtained in the case of flow due to porous plates rotating with the same constant angular velocity about a common axis (Rajagopal 1984) and also in the case of a certain class of non-Newtonian fluids (Rajagopal 1982).

For the form of the velocity field sought, it is found that the set of governing equations contains the nonlinear equations of axisymmetric flow and two coupled linear equations, the coefficients of which depend on the solution of the axisymmetric problem. Thus whenever there is a numerical solution to the Kármán problem, we can proceed to determine the asymmetric solution numerically, by virtue of the analysis of Parter & Rajagopal (1984).

In this paper we present asymmetric solutions for both coincident and non-coincident axes of rotation at two values of the Ekman number $E = \frac{1}{100}$ and $\frac{1}{275}$ and at relative disk rotations $s = 0.8$, 0 and -0.25.

The streamlines of the Kármán flow $\{F, G, H\}$ are equiangular spirals in each $z =$ constant plane, cutting the radius at the angle $\tan^{-1}[G(z)/F(z)]$. The asymmetric flow that is investigated here is the result of superposition, in each $z =$ constant plane, of the Kármán flow and a rigid-body translation, the translation, however, being different from plane to plane. In midplane the translational velocity is arbitrary: when made non-dimensional with $(\nu\omega)^{\frac{1}{2}}$ its Cartesian components are $\{0, -C\}$, where C is an arbitrary constant. In other $z =$ constant planes the non-dimensional translational velocity has Cartesian components $\{g(z), -f(z)\}$. The functions $g(z)$ and $f(z)$ are defined by variable-coefficient linear ordinary differential equations, the coefficients of which depend on the Kármán solution $\{G(z), F(z)\}$ and on the constant C. Thus symmetric solutions of the Kármán problem are never isolated when considered within the scope of the full Navier–Stokes equations; there are asymmetric solutions in every neighbourhood of the Kármán solutions.

The asymmetric flow under discussion possesses, in each $z =$ constant plane, a point of stagnation. The distance between the axis of rotation and the stagnation point depends, for a given Kármán flow, on the value of the constant C. The locus of the stagnation points is a three-dimensional curve with endpoints on the axis of rotation at the disks, or, in the case of distinct axes, on the axes of rotation where those intersect the disks. Stagnation here is defined by $u = v = 0$.

2. Governing equations

The flow field is bounded by two parallel disks of infinite radii, located at $x^3 = 0$ and $x^3 = d$ respectively in the cylindrical polar coordinate system $\{x^1, x^2, x^3\}$. We define another, non-dimensional, coordinate system $\{r, \theta, z\}$, where $r = x^1/d$, $\theta = x^2$ and $z = x^3/d$.

The classical assumptions for the velocity field for flow of an incompressible Newtonian fluid between the disks rotating about coincident axes with constant (but differing) angular velocity $\omega_1 = \omega$ and $\omega_2 = s\omega$, can be written as

$$u = x^1\omega\, F(z), \quad v = x^1\omega\, G(z), \quad w = d\omega\, E^{\frac{1}{2}} H(z). \tag{1}$$

Here $\boldsymbol{v} = \{u, v, w\}$ is the velocity and E is the Ekman number. The velocity satisfies the constraint

$$\operatorname{div} \boldsymbol{v} = 0, \tag{2}$$

provided that we allow

$$F(z) = -\tfrac{1}{2}E^{\frac{1}{2}}H'. \tag{3}$$

Under the assumptions (1) and (3) the Navier–Stokes equations reduce to

$$E^{\frac{1}{2}}H^{\mathrm{iv}} - HH''' - 4E^{-1}GG' = 0, \quad E^{\frac{1}{2}}G'' + H'G - G'H = 0. \tag{4a,b}$$

The appropriate boundary conditions are

$$H(0) = H'(0) = 0, \quad G(0) = 1, \quad H(1) = H'(1) = 0, \quad G(1) = s. \tag{5a,b}$$

In this paper we follow Parter & Rajagopal (1984) and seek solutions to the equations of motion and continuity in the more general form:†

$$u = x^1\omega\{F(z) + \frac{1}{r}E^{\frac{1}{2}}[g(z)\cos\theta - f(z)\sin\theta]\}, \tag{6a}$$

$$v = x^1\omega\{G(z) - \frac{1}{r}E^{\frac{1}{2}}[g(z)\sin\theta + f(z)\cos\theta]\}, \tag{6b}$$

$$w = d\omega E^{\frac{1}{2}}H(z). \tag{6c}$$

If $H = 0$ and $G = 1$ we have a velocity field of the form described by Berker (1979). And, if $f = 0$ and $g = 0$, we recover Kármán's (1921) assumption.

The incompressibility constraint (2) again leads to the condition (3), but now the Navier–Stokes equations yield a set of four ordinary differential equations:

$$E^{\frac{1}{2}}H''' - HH'' + \tfrac{1}{2}H'^2 - 2E^{-1}G^2 + 2E^{-1}k = 0, \quad E^{\frac{1}{2}}G'' + H'G - HG' = 0, \tag{7a,b}$$

$$E^{\frac{1}{2}}f''' - Hf'' - \tfrac{1}{2}H'f' + \tfrac{1}{2}H''f + E^{-\frac{1}{2}}(Gg)' = 0,$$

$$E^{\frac{1}{2}}g''' - Hg'' - \tfrac{1}{2}H'g' + \tfrac{1}{2}H''g - E^{-\frac{1}{2}}(Gf)' = 0. \tag{7c,d}$$

The boundary conditions are

$$H(0) = H'(0) = 0, \quad G(0) = 1, \tag{8a}$$

$$f(0) = 0, \quad g(0) = -\kappa E^{-\frac{1}{2}}, \tag{8b}$$

$$H(1) = H'(1) = 0, \quad G(1) = s, \tag{8c}$$

$$f(1) = 0, \quad g(1) = s\kappa E^{-\frac{1}{2}}, \tag{8d}$$

$$f(\tfrac{1}{2}) = C, \quad g(\tfrac{1}{2}) = 0. \tag{8e}$$

Here C is a non-dimensional arbitrary constant and $\kappa = a/2d$ is the non-dimensional distance between the (non-coincident) axes of rotation. Also note that (7a) is obtained from (4a) by integration, k being the integration constant. k is also the eigenvalue of the boundary-value problem (7), (8).

Parter & Rajagopal (1984) show that whenever there is a solution to the Kármán problem (7a, b), (8a,c) there is also a solution of the system (7c,d), (8b,d,e) for each C. Thus symmetric solutions of the problem of flow between parallel plates rotating about a common axis or about distinct axes are never isolated: there are asymmetric solutions arbitrarily close by.

For $\kappa = 0$ and $s = 1$ the above set of equations represents a one-parameter, viz C, family of solutions for asymmetric flow between disks rotating about a common axis. The symmetric component of the flow is rigid-body motion when $H(z) = 0$ and $G(z) = 1$. In this case (7c,d) reduce to

$$f''' + E^{-1}g' = 0, \quad g''' - E^{-1}f' = 0, \tag{9a,b}$$

† We adopt here the nomenclature of Holodniok *et al.* (1977), as being more convenient for comparison with the existing numerical work.

with boundary conditions from (8),

$$f(0) = g(0) = 0; \quad f(1) = g(1) = 0, \tag{10a}$$

and the midpoint conditions

$$f(\tfrac{1}{2}) = C, \quad g(\tfrac{1}{2}) = 0. \tag{10b}$$

Equations (9) and (10) were first given by Berker (1979), who also published the exact solutions to these equations. Thus rigid-body motion is imbedded in Berker's class of solutions and is given by $C = 0$. Berker's solutions correspond to flows such that in any $z =$ constant plane the streamlines are concentric circles. The locus of the centre of these concentric circles is given by $x = f(z)$ and $y = g(z)$, where $\{x, y, z\}$ are non-dimensional orthogonal Cartesian co-ordinates located in the axis of rotation, so that the locus of the centre of rotations intersect the $z = \frac{1}{2}$ plane at the point $\{C, 0, \frac{1}{2}\}$. The flow field is a special subclass of the pseudoplane flows which have been studied by Berker (1936). When $F(z) = 0$, $G(z) = 1$ and the velocity field is given by (6), the flow is the superposition of Berker's solution and the rigid-body rotation of the Kármán problem; the point $\{C, 0, \frac{1}{2}\}$ in this case moves on a closed circular path with velocity $Cd\omega$.

3. Numerical method

We intend to approximate $\{H(z), G(z), f(z), g(z)\}$, which is given only implicitly as solutions of (7) and (8), by piecewise polynomial functions. Thus, following de Boor (1978), we partition the interval $[0, 1]$ as

$$\pi: 0 = z_1 < z_2 < \ldots < z_l < z_{l+1} = 1.$$

Let $p_1(z), \ldots, p_l(z)$ be any sequence of l polynomials, each of order k (i.e. of degree $< k$), and denote the collection of all piecewise polynomial functions $h(z)$ by $P_{k,\pi}$.

$$P_{k,\pi} = \{h(z): h(z) = p_i(z) \text{ if } z \in [z_i, z_{i+1}],\ 1 \leqslant i \leqslant l\}. \tag{11}$$

$P_{k,\pi}$ is a linear space, and since there are l subintervals the dimension of $P_{k,\pi}$ is kl. Consider now subspaces $S_{k,\pi,\nu}$, of $P_{k,\pi}$ generated by imposing smoothness constraints on elements of $P_{k,\pi}$ at the interior breakpoints z_i, $2 \leqslant i \leqslant l$. Let $\nu = \{\nu_i\}_{i=2}^{l}$ be a non-negative integer sequence, with $\nu_i \leqslant k$, all i, where ν_i denotes the smoothness index of the piecewise polynomial subspace $S_{k,\pi,\nu}$ at the breakpoint z_i, so that $h^{(j)}(z_i^+) = h^{(j)}(z_i^-)$, $0 \leqslant j \leqslant \nu_i - 1$. Then the dimension N of the subspace $S_{k,\pi,\nu}$ is given by

$$\dim S_{k,\pi,\nu} = k + \sum_{i=2}^{l} (k - \nu_i). \tag{12}$$

We now construct a basis for $S_{k,\pi,\nu}$ such that each element of the basis has local support and each element is non-negative.

The space $S_{k,\pi,\nu}$ is a space of polynomial splines, and a basis of the above type is called a B-spline basis. To generate such a basis, we consider divided differences of order k of the truncated power function $(z-t)_+^{k-1} = \max[(z-t)^{k-1}, 0]$. But direct evaluation of the B-spline B_i from its definition is unsatisfactory, e.g. there is loss of significance during computation. It is more expedient to employ the recurrence relation (de Boor 1978)

$$\left.\begin{aligned} B_{i,k}(z) &= \frac{z - t_i}{t_{i+k-1} - t_i} B_{i,k-1}(z) + \frac{t_{i+k} - z}{t_{i+k} - t_{i+1}} B_{i+1,k-1}(z), \\ B_{j,1}(z) &= \begin{cases} 1 & \text{for} \quad z \in [t_j, t_{j+1}], \\ 0 & \text{otherwise.} \end{cases} \end{aligned}\right\} \tag{13}$$

Here $t = \{t_i\}_{i=1}^{N+k}$ is any non-decreasing sequence such that

(i) $t_1 \leqslant t_2 \leqslant \ldots \leqslant t_k \leqslant z_1$ and $z_{l+1} \leqslant t_{N+1} \leqslant \ldots \leqslant t_{N+k}$;

(ii) the number $z_i, 2 \leqslant i \leqslant l$, occurs exactly $d_i = k - \nu_i$ times in t.

The sequence $B_1, B_2, \ldots, B_N$ of B-splines of order k for the knot sequence t is a basis for $S_{k,\pi,\nu}$, according to the Curry–Schoenberg theorem. The choice of t translates the desired amount of smoothness at a breakpoint z_i, and the theorem permits construction of a B-spline basis for any particular piecewise polynomial space $S_{k,\pi,\nu}$.

The B-splines thus defined provide a partition of unity:

$$\left.\begin{aligned} B_i(z) \geqslant 0, \quad 1 \leqslant i \leqslant N, \\ \sum_{i=1}^{N} B_i(z) = 1 \end{aligned}\right\} \quad \forall z \in [z_1, z_{l+1}]. \tag{14a}$$

Other relevant properties of B-splines are

$$\left.\begin{aligned} B_1(z_1) = B_N(z_{l+1}) = 1, \qquad B_j(z_1) = 0 \quad (j > 1), \\ B_j(z_{l+1}) = 0 \quad (j < N), \qquad B_j(z) = 0 \quad (z \notin [t_j, t_{j+k}]) \end{aligned}\right\} \tag{14b}$$

$$\left.\begin{aligned} B_1'(z_1) = -B_2'(z_1) \neq 0, \qquad B_j'(z_1) = 0 \quad (j > 2), \\ B_N'(z_{l+1}) = -B_{N-1}'(z_{l+1}) \neq 0, \qquad B_j'(z_{l+1}) = 0 \quad (j < N-1). \end{aligned}\right\} \tag{14c}$$

In the present calculations we employ a cubic B-spline basis, $k = 4$, and a knot sequence

$$\left.\begin{aligned} z_1 = t_1 = t_2 = t_3 = t_4, \\ z_2 = t_5, \\ \vdots \\ z_l = t_N, \\ z_{l+1} = t_{N+1} = t_{N+2} = t_{N+3} = t_{N+4}, \end{aligned}\right\} \tag{15}$$

and seek solutions of (7) in the weak form

$$\left.\begin{aligned} H(z) = \sum_{i=1}^{N} H_i B_i(Z), \quad G(z) = \sum_{i=1}^{N} G_i B_i(z), \\ f(z) = \sum_{i=1}^{N} f_i B_i(z), \quad g(z) = \sum_{i=1}^{N} g_i B_i(z). \end{aligned}\right\} \tag{16}$$

These expansions can be forced to satisfy the boundary conditions (8a,b) in the strong form via the spline properties (14). This yields

$$\left.\begin{aligned} H(z) = \sum_{n=3}^{N-2} H_n B_n(z), \quad G(z) = B_1(z) + sB_N(z) + \sum_{n=2}^{N-1} G_n B_n(z), \\ f(z) = \sum_{n=2}^{N-1} f_n B_n(z), \quad g(z) = \kappa E^{-\frac{1}{2}}[sB_N(z) - B_1(z)] + \sum_{n=2}^{N-1} g_n B_n(z), \end{aligned}\right\} \tag{17}$$

while the midpoint conditions (8c) assume the form

$$\sum_{n=2}^{N-1} f_n B_n(\tfrac{1}{2}) = C, \quad \sum_{n=2}^{N-1} g_n B_n(\tfrac{1}{2}) = 0. \tag{18}$$

In the application of Galerkin's method, the expansions (17) are substituted into (7).

The resulting equations are multiplied through by the test sets $\tau^{\mathrm{H}}, \tau^{\mathrm{G}}, \tau^{\mathrm{f}}$ and τ^{g} respectively:

$$\left.\begin{aligned} \tau^{\mathrm{H}} &= \{B_i(z)\colon 3 \leqslant i < N-1\}, \quad \tau^{\mathrm{G}} = \{B_j(z)\colon 2 \leqslant j \leqslant N-1\}, \\ \tau^{\mathrm{f}} &= \{B_k(z)\colon 2 \leqslant k \leqslant N-2\}, \quad \tau^{\mathrm{g}} = \{B_l(z)\colon 2 \leqslant l \leqslant N-2\}. \end{aligned}\right\} \tag{19}$$

Integration over the domain $0 \leqslant z \leqslant 1$ leads to the following nonlinear algebraic system:

$$\sum_{i=1}^{N} \{-H_i \bar{z}_{li}^{(4)} + 2E^{-\frac{3}{2}} k \bar{z}_{li}^{(0)}\} + \sum_{i=1}^{N}\sum_{j=1}^{N} \{-2E^{-\frac{3}{2}} G_i G_j \bar{Z}_{lij}^{(0)} + E^{-\frac{1}{2}} H_i H_j (\tfrac{1}{2}\bar{Z}_{lij}^{(3)} - \bar{Z}_{lij}^{(2)})\} = 0, \tag{20a}$$

$$\sum_{i=1}^{N} G_i \bar{z}_{mi}^{(2)} + E^{-\frac{1}{2}} \sum_{i=1}^{N}\sum_{j=1}^{N} H_j G_i (\bar{Z}_{mij}^{(1)} - \bar{Z}_{mji}^{(1)}) = 0, \tag{20b}$$

$$\sum_{j=1}^{N} \left\{-E^{-\frac{1}{2}} \bar{z}_{nj}^{(4)} + \sum_{i=1}^{N} H_i (\tfrac{1}{2}\bar{Z}_{nji}^{(2)} - \tfrac{1}{2}\bar{Z}_{nij}^{(3)} - \bar{Z}_{nij}^{(2)})\right\} f_j + E^{-\frac{1}{2}} \sum_{i=1}^{N}\sum_{j=1}^{N} G_i (\bar{Z}_{nij}^{(1)} + \bar{Z}_{nji}^{(1)}) g_j = 0, \tag{20c}$$

$$-E^{-\frac{1}{2}} \sum_{i=1}^{N}\sum_{j=1}^{N} G_i (\bar{Z}_{pij}^{(1)} + \bar{Z}_{pji}^{(1)}) f_j - \sum_{j=2}^{N-1} \left\{E^{\frac{1}{2}} \bar{z}_{pj}^{(4)} + \sum_{i=1}^{N} H_i (\bar{Z}_{pij}^{(2)} + \tfrac{1}{2}\bar{Z}_{pij}^{(3)} - \tfrac{1}{2}\bar{Z}_{pji}^{(2)})\right\} g_j = 0 \tag{20d}$$

$$(2 \leqslant l \leqslant N-2, \quad 2 < m \leqslant N-1, \quad 2 \leqslant n \leqslant N-2, \quad 2 \leqslant p \leqslant N-2).$$

Implicit in (20) is that

$$\left.\begin{aligned} H_1 = H_2 = H_N = H_{N-1} = 0, \quad G_1 = 1, \quad G_N = s, \\ f_1 = f_N = 0, \quad g_1 = -\kappa E^{-\frac{1}{2}}, \quad g_N = s\kappa E^{-\frac{1}{2}}. \end{aligned}\right\} \tag{21}$$

The Galerkin coefficients $\bar{z}_{jk}^{(0)}, \ldots, \bar{Z}_{ijk}^{(3)}$ are defined as follows:

$$\left.\begin{aligned} \bar{z}_{jk}^{(\alpha)} &= \int_0^1 B_j^{(b)}(z)\, B_k^{(c)}(z)\, \mathrm{d}z, \\ \bar{Z}_{ijk}^{(\alpha)} &= \int_0^1 B_i^{(a)}(z)\, B_j^{(b)}(z)\, B_k^{(c)}(z)\, \mathrm{d}z \quad (a \leqslant b < c), \end{aligned}\right\} \tag{22}$$

$$\alpha = a+b+c+1 \text{ (if } b \neq 0), +2 \text{ (if } a \neq 0).$$

The nonlinear algebraic system consisting of (18), (20) and (21) is solved via a Newton-like method on the PDP-10 of the University of Pittsburgh.

The accuracy of the Galerkin B-spline formulation has been discussed elsewhere (Szeri *et al.* 1983*a*; Szeri & Giron 1984). Here we report on two studies. At $E^{-1} = 100$ the equations of axisymmetric flow (7*a*, *b*) seem to possess a unique solution, leading to a unique value of the constant k (Holodniok *et al.* 1977). We calculated this solution for various dimensions N of the approximating subspace. The resulting k-values are shown in table 1. In tables 2 and 3 we display solutions for $f(z)$ and $g(z)$ obtained at $E^{-1} = 275$ and $F(z) = 0$, $G(z) = 1.0$, corresponding to rigid-body rotation of the axisymmetric component of the flow. The solutions reported here are the exact solution of Berker (1979), and our numerical solutions of (7) at $N = 43$ and 63

N	k
13	0.802886
23	0.803891
33	0.803961
43	0.803977
63	0.803986

TABLE 1. Dependence of k on N ($E^{-1} = 100$, $s = 0.8$, $\kappa = 0$)

		Numerical	
z	Exact (Berker 1979)	$N = 43$	$N = 63$
0	0.00000	0.00000	0.00000
0.1	0.883899	0.883897	0.883899
0.2	1.07250	1.07250	1.07250
0.3	1.03307	1.03307	1.03307
0.4	1.00479	1.00479	1.00479
0.5	1.00000	1.00000	1.00000

TABLE 2. Comparison of solutions: $f(z)$ ($E^{-1} = 275$, $F = 0$, $G = 1, C = 1, \kappa = 0$)

		Numerical	
z	Exact (Berker 1979)	$N = 43$	$N = 63$
0	0.000000	0.000000	0.000000
0.1	0.288866	0.288867	0.288864
0.2	0.071361	0.071362	0.071359
0.3	−0.008291	−0.008291	−0.008292
0.4	−0.006282	−0.006282	−0.006282
0.5	0.000000	0.9095×10^{-12}	-0.4547×10^{-12}

TABLE 3. Comparison of solutions: $g(z)$ ($E^{-1} = 275$, $F = 0$, $G = 1$, $C = 1$, $\kappa = 0$)

respectively. The numerical solutions at $N = 63$ displays a better than 5-digit accuracy, which we consider as adequate.

The calculations reported in this paper were all performed with $N = 63$ in (7), leading to a 243-equation mathematical model of the flow in (7).

4. Results and discussion

4.1. *Common axis of rotation*

The calculations reported here were performed with relative disk rotations $s = 0.8$, 0 and -0.25 at two values of the Ekman number $E = \frac{1}{100}$ and $\frac{1}{275}$.

Figure 1 shows the locus of stagnation points Γ for Berker's (1979) solution at $E = \frac{1}{275}$. This curve is defined by $x = f(z)$, $y = g(z)$, and Γ_{xy} is its projection onto the (x, y)-plane. Γ is the centre of concentric circles, in each z = constant plane, which are the streamlines of Berker's flow between corotating disks.

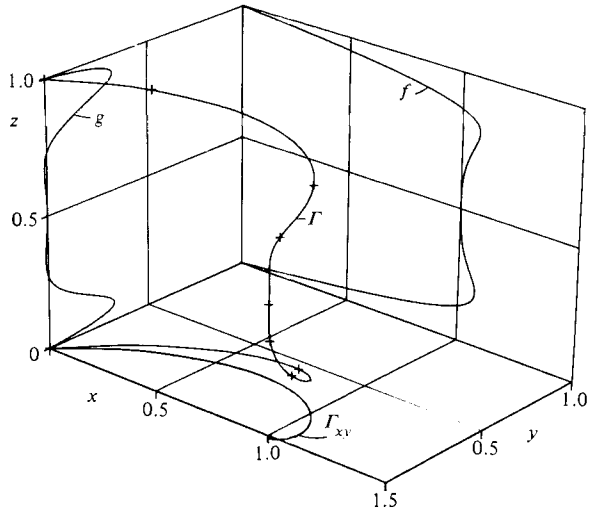

FIGURE 1. Locus of stagnation points; Berker's solution, $E = \frac{1}{275}$, $s = 1$ ($\Gamma \equiv$ locus, $\Gamma_{xy} \equiv$ projection onto (x, y)-plane).

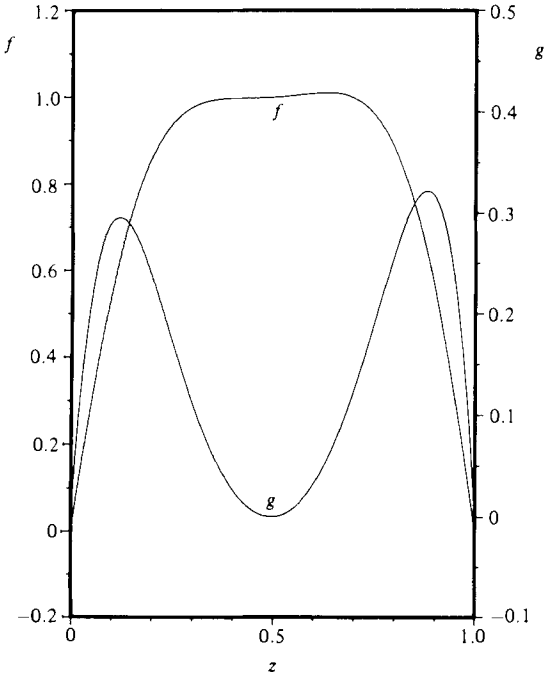

FIGURE 2. Branch I at $E = \frac{1}{100}$, $s = 0.8$, $\kappa = 0$, $C = 1$.

At $E = \frac{1}{100}$ and $s = 0.8$ we find the Holodniok *et al.* (1971) solution to the Kármán problem (4*a*, *b*). The corresponding $f(z)$ and $g(z)$ functions obtained at $C = 1$ are shown plotted in figure 2, while the complete solution is contained in table 4. The functions $f(z)$ and $g(z)$ show a fair degree of symmetry about the $z = \frac{1}{2}$ plane and when added to the Kármán solution at $\theta = \frac{1}{4}\pi$ (the position $\theta = 0$ being arbitrary) and at various radial positions, $r = \infty, 10, 1$, they produce the dimensionless velocity

z	F	G	H	f	g
0	0	1.000000	0.000000	0.000000	0.000000
0.1	0.314395×10^{-1}	0.919384	-0.492656×10^{-1}	0.549652	0.290994
0.2	0.135604×10^{-1}	0.892197	-0.953676×10^{-1}	0.864356	0.234692
0.3	0.155853×10^{-2}	0.891471	−0.108498	0.978326	0.110850
0.4	-0.898241×10^{-3}	0.894725	−0.108083	0.997869	0.259424×10^{-1}
0.5	0.366803×10^{-3}	0.896623	−0.107312	1.000000	1.181899×10^{-11}
0.6	0.145854×10^{-2}	0.898954	−0.109446	1.009070	0.324630×10^{-1}
0.7	-0.181262×10^{-2}	0.902919	−0.110300	0.996678	0.125329
0.8	-0.148588×10^{-1}	0.901788	−0.954889	0.882594	0.258369
0.9	-0.314345×10^{-1}	0.874096	−0.475105	0.558464	0.316277
1.0	0	0.8	0	0.000000	0.000000

TABLE 4. Branch I at $E^{-1} = 100$ ($N = 63$, $s = 0.8$, $C = 1$, $\kappa = 0$)

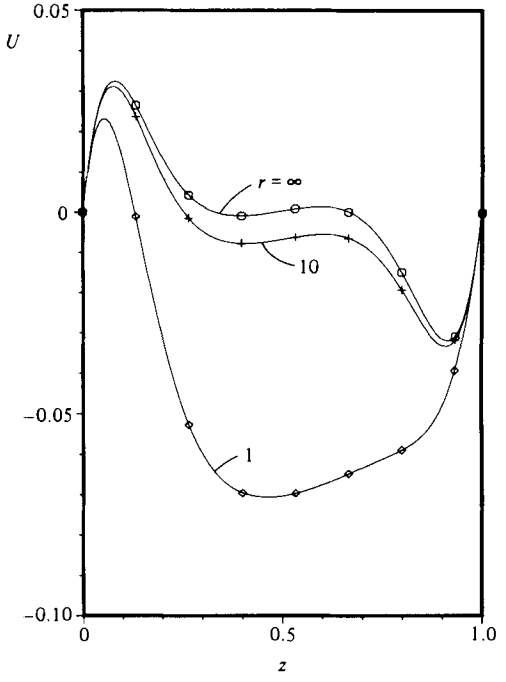

FIGURE 3. Radial component of non-dimensional velocity, $U = u/x^1\Omega$; branch I, at $E = \frac{1}{100}$, $s = 0.8$, $\kappa = 0$, $C = 1$, $\theta = \frac{1}{4}\pi$.

components $U = u/x^1\omega$ and $V = v/x^2\omega$ of figures 3 and 4. As $r \to \infty$ the flow is the axisymmetric Kármán flow, indicating a boundary-layer structure of the Batchelor type (Batchelor 1951). The core tangential velocity is intermediate between the rotational velocities of the two disks. The radial component of the velocity is almost antisymmetric with respect to the channel centreline: the fluid adjacent to the fast disk is thrown outward, the core velocity is almost zero and return flow occurs at the slow disk. This flow picture changes significantly upon moving inwards, towards the centre of rotation. The core acquires a constant radial velocity with decreasing r (figure 3), while its tangential velocity slows down almost to the rotational velocity

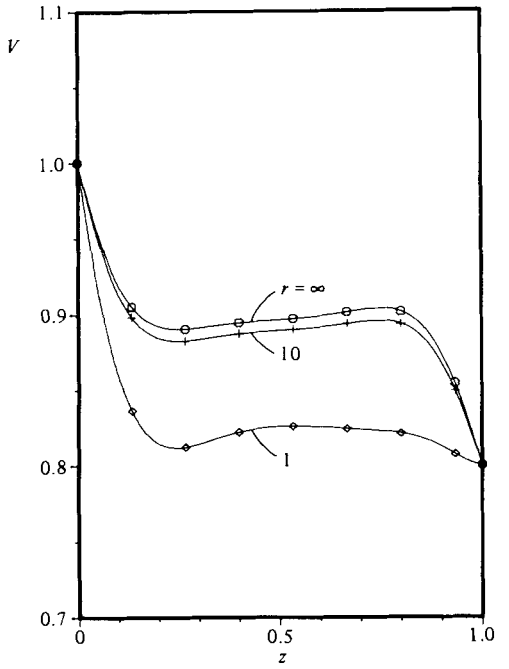

FIGURE 4

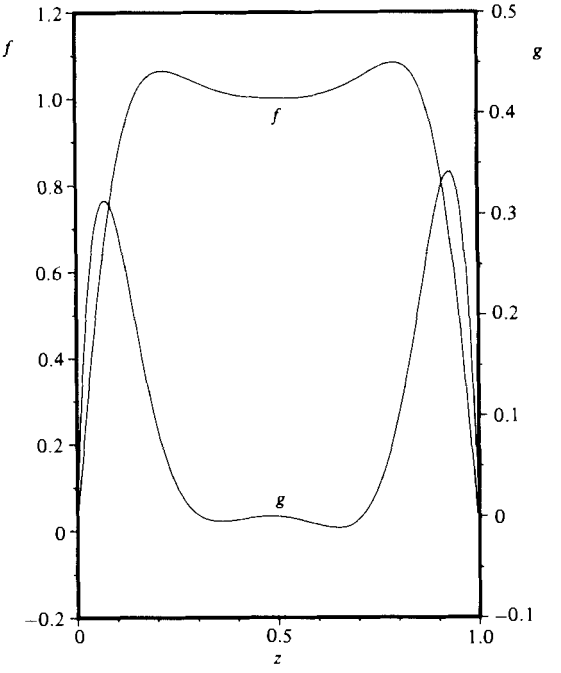

FIGURE 5

FIGURE 4. Tangential component of non-dimensional velocity $V = v/x^1\Omega$: branch I at $E = \frac{1}{100}$, $s = 0.8$, $\kappa = 0$, $C = 1$, $\theta = \frac{1}{4}\pi$.

FIGURE 5. Branch I at $E = \frac{1}{275}$; $s = 0.8$, $\kappa = 0$, $C = 1$.

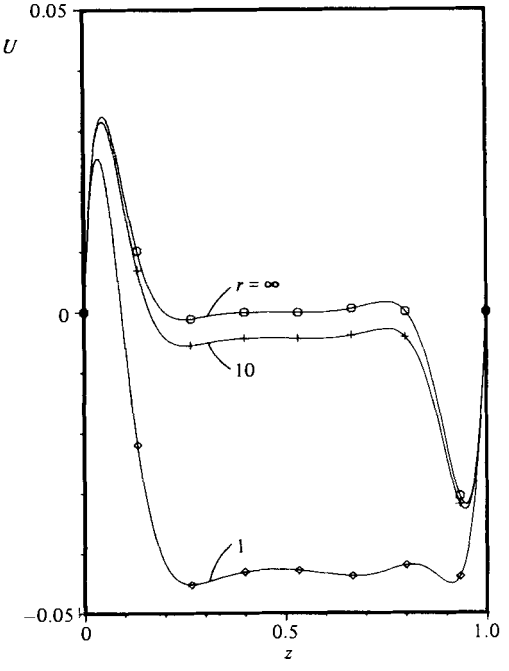

FIGURE 6

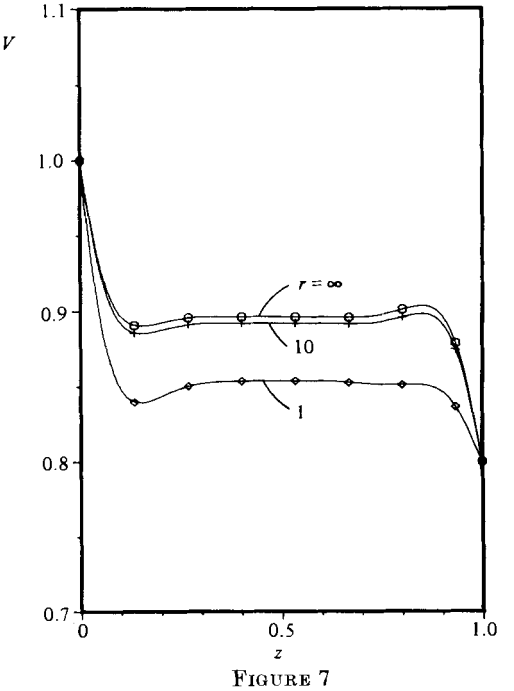

FIGURE 7

FIGURE 6. Radial component of non-dimensional velocity $U = u/x^1\Omega$; branch I at $E = \frac{1}{275}$, $s = 0.8$, $\kappa = 0$, $C = 1$, $\theta = \frac{1}{4}\pi$.

FIGURE 7. Tangential component of non-dimensional velocity $V = v/x^1\Omega$; branch I at $E = \frac{1}{275}$, $s = 0.8$, $\kappa = 0$, $C = 1$, $\theta = \frac{1}{4}\pi$.

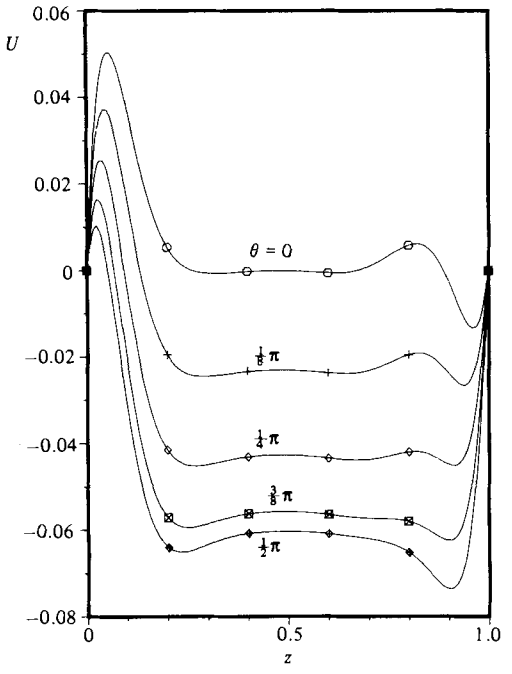

FIGURE 8

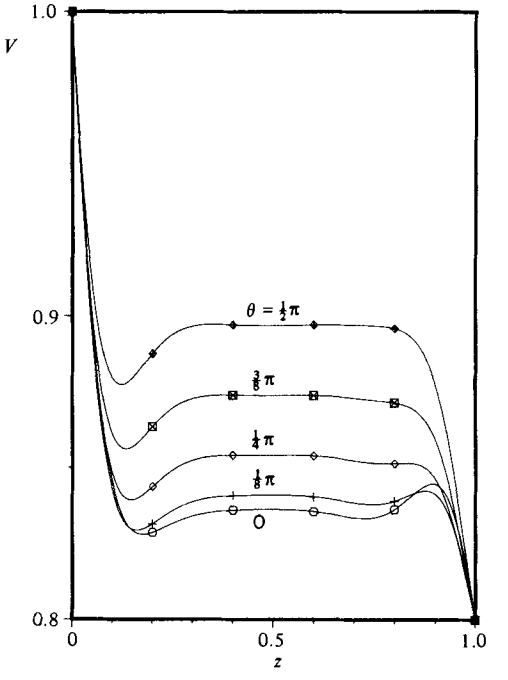

FIGURE 9

FIGURE 8. Development of radial component of non-dimensional velocity $U = u/x^1\Omega$; branch I at $E = \frac{1}{275}$, $r = 1.0$, $s = 0.8$, $\kappa = 0$, $C = 1$.

FIGURE 9. Development of tangential component of non-dimensional velocity $V = v/x^1\Omega$; branch I at $E = \frac{1}{275}$, $r = 1.0$, $s = 0.8$, $\kappa = 0$, $C = 1$.

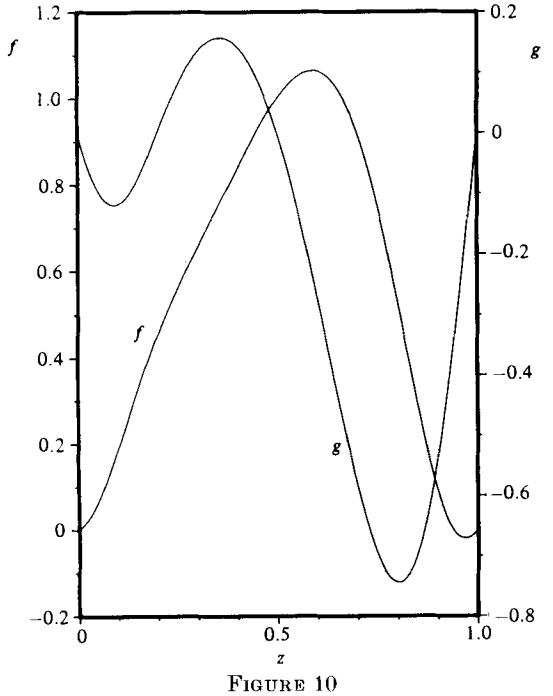

FIGURE 10

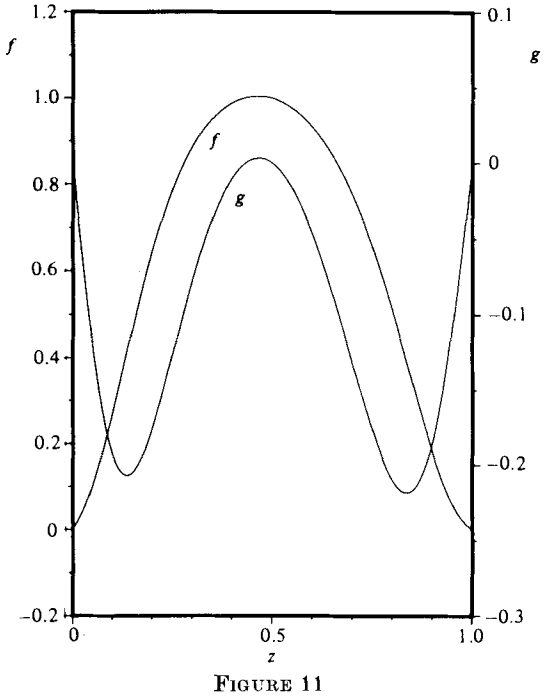

FIGURE 11

FIGURE 10. Branch II at $E = \frac{1}{275}$, $s = 0.8$, $\kappa = 0$, $C = 1$.

FIGURE 11. Branch IV at $E = \frac{1}{275}$, $s = 0.8$, $\kappa = 0$, $C = 1$.

of the slow disk (figure 4). There is, of course, an infinity of solutions, one for each value of C.

The Kármán problem seems to possess three distinct solutions at $E^{-1} = \frac{1}{275}$ and $s = 0.8$, as already reported by Holodniok *et al.* (1977). These solutions are identified by Holodniok *et al.* as branches I, II and IV.

Branch I at $E = \frac{1}{275}$ is not unlike the solution already discussed at $E = \frac{1}{100}$. (In fact these two solutions are of the same branch, as may be shown by continuation in E.) But the boundary-layer structure is more pronounced at $E^{-1} = 275$, as may be seen from figures 6 and 7 at $r \to \infty$. The corresponding $f(z)$ and $g(z)$ at $C = 1$ are plotted in figure 5. When these functions are superposed on the Kármán solution at $\theta = \frac{1}{4}\pi$, $C = 1$ and various non-dimensional radial positions r, we obtain figure 6 for non-dimensional radial velocity and figure 7 for non-dimensional tangential velocity. At $r \to \infty$ the flow is, again, the symmetric Kármán flow: the core radial velocity is almost uniformly zero and there are two boundary layers, one at the fast disk (outflow) and the other at the slow disk (inflow). The core rotates uniformly at what appears to be the mean disk angular velocity. On moving inwards along the radius $\theta = \frac{1}{4}\pi$, the core acquires an inward velocity and its rotation is slowed to close to the angular velocity of the slow disk. Figures 8 and 9 indicate the development of the velocity profile when the observer is moving along the unit circle $r = 1$. From $\theta = 0$ the position $\theta = 0$ being arbitrary, moving in the direction of increasing θ we find that the core, which had negligible radial velocity at $\theta = 0$, acquires an inward velocity and its rotation is speeded up towards the mean angular velocity of the disks. From $\theta = \frac{1}{2}\pi$ onward, the trend changes: the core loses its inward velocity but its rotational velocity keeps increasing. In the third quarter, $\pi \leqslant \theta \leqslant \frac{3}{2}\pi$, still moving in the positive direction, increasing θ results in a strengthening of the radial outflow and in a weakening of the core's rotation. For $\theta \in (\frac{3}{2}\pi, 2\pi)$ the radial outward velocity of the core is lost and its rotation is retarded gradually, as θ increases. Development of the boundary layers may similarly be discussed.

The other two solutions of the Kármán problem obtained at $E = \frac{1}{275}$, $s = 0.8$, result in $f(z)$ and $g(z)$, with $C = 1$, as shown in figure 10 for branch II and figure 11 for branch IV. The corresponding non-dimensional velocity profiles are displayed in figures 12–15. The physical interpretation of these two branches is not obvious. These solutions are of 'two-cell' type, where a cell is identified as a region that is bounded by $z =$ constant planes on which the axial velocity vanishes (Nguyen *et al.* 1975). Neither the radial nor the tangential velocity seem to vary in a qualitative sense on moving inwards from $r = \infty$, along the radius $\theta = \frac{1}{4}\pi$. At any rate, these solutions were found to be unstable to infinitesimal disturbances at all radial positions (Szeri *et al.* 1983*a*), and are thus not thought to be easily reproducible in the laboratory.

In figures 16–18 we present solutions for one stationary disk $s = 0$ at $E = \frac{1}{275}$. These were obtained by continuation in s from the previously discussed $s = 0.8$, branch I solution. Figure 16 displays the functions $f(z)$ and $g(z)$, calculated with $C = 1$. The non-dimensional radial velocity is shown in figure 17, indicating almost no boundary-layer structure. There is more of a core in evidence when plotting tangential velocity, as in figure 18. There is little qualitative change in either U or V when moving from $r = \infty$ inwards, along the line $\theta = \frac{1}{4}\pi$, towards the axis of rotation.

At $s = 1$ branch I supplies only the trivial (rigid-body) solution (Holodniok *et al.* 1981). The functions $f(z)$ and $g(z)$ were already given by Berker (1979), and are recorded in tables 2 and 3.

Continuation in s is time-consuming.† In the interval $0.8 > s > 0$ we were forced

† By continuation we mean the procedure whereby the solution obtained at $s = s_0$ is used to start the Newton iteration at $s = s_0 + \Delta s$.

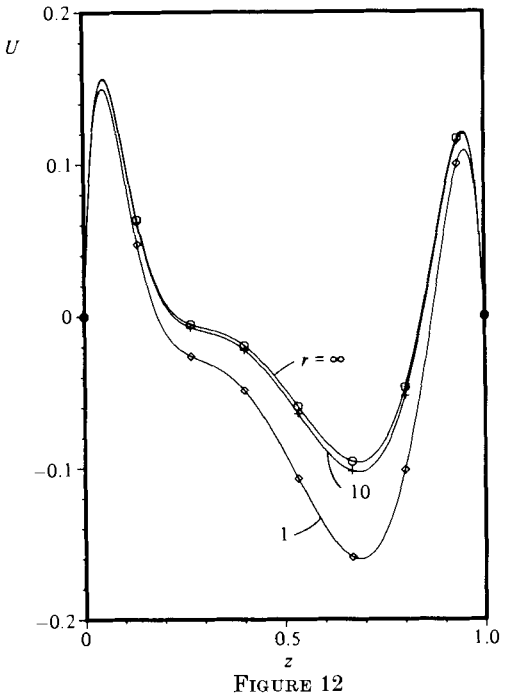

FIGURE 12

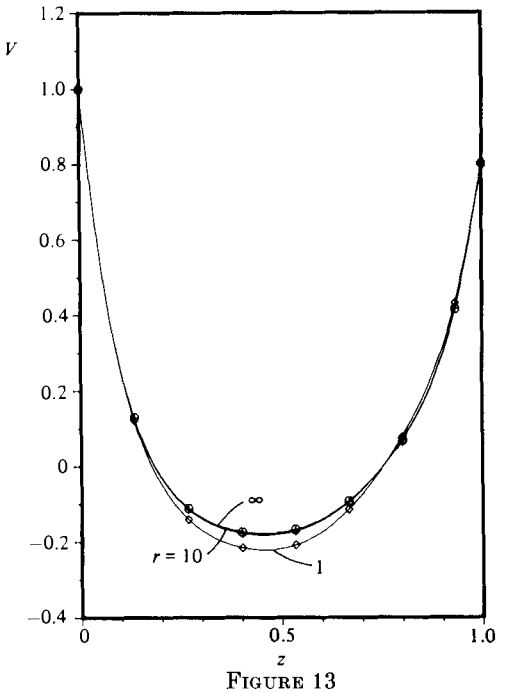

FIGURE 13

FIGURE 12. Radial component of non-dimensional velocity $U = u/x^1\Omega$; branch II at $E = \frac{1}{275}$, $s = 0.8$, $\kappa = 0$, $C = 1$, $\theta = \frac{1}{4}\pi$.

FIGURE 13. Tangential velocity component of non-dimensional velocity $V = v/x^1\Omega$; branch II at $E = \frac{1}{275}$, $s = 0.8$, $\kappa = 0$, $C = 1$, $\theta = \frac{1}{4}\pi$.

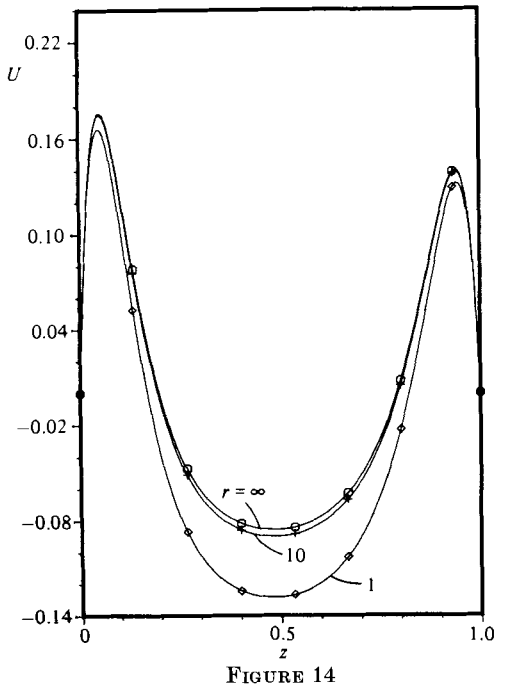

FIGURE 14

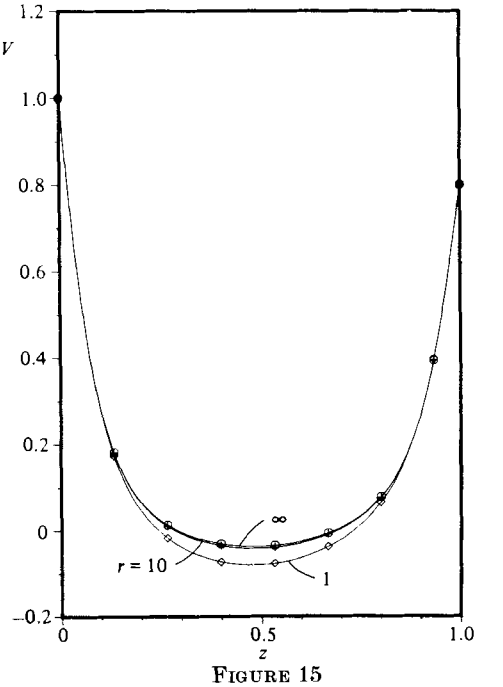

FIGURE 15

FIGURE 14. Radial component of non-dimensional velocity $U = u/x^1\Omega$; branch IV at $E = \frac{1}{275}$, $s = 0.8$, $\kappa = 0$, $C = 1$, $\theta = \frac{1}{4}\pi$.

FIGURE 15. Tangential component of non-dimensional velocity $V = v/x^1\Omega$; branch IV at $E = \frac{1}{275}$, $s = 0.8$, $\kappa = 0$, $C = 1$, $\theta = \frac{1}{4}\pi$.

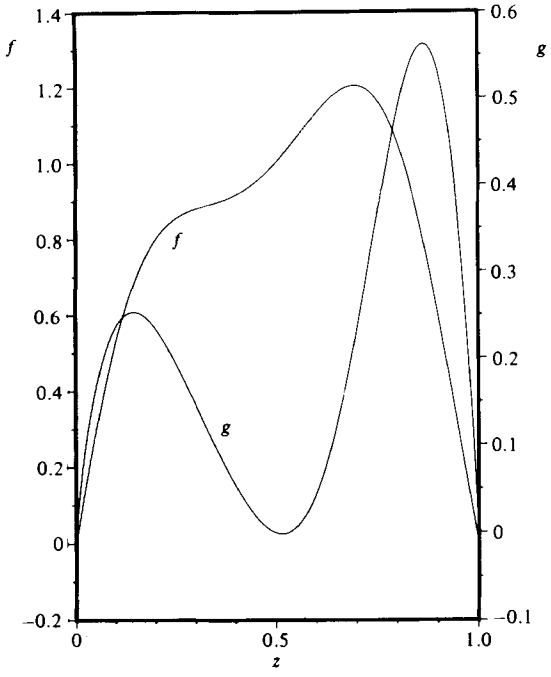

FIGURE 16

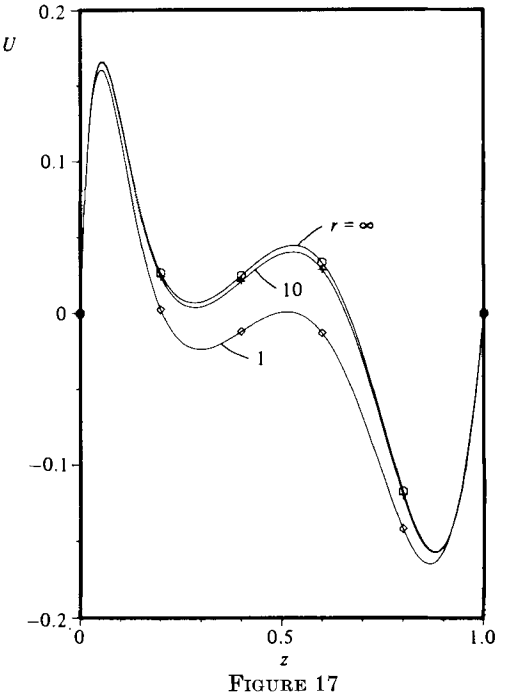

FIGURE 17

FIGURE 16. Branch I at $E = \frac{1}{275}$, $s = 0$, $\kappa = 0$, $C = 1$.

FIGURE 17. Radial component of non-dimensional velocity $U = u/x^1\Omega$; branch I at $E = \frac{1}{275}$, $s = 0$, $\kappa = 0$, $C = 1$, $\theta = \frac{1}{4}\pi$.

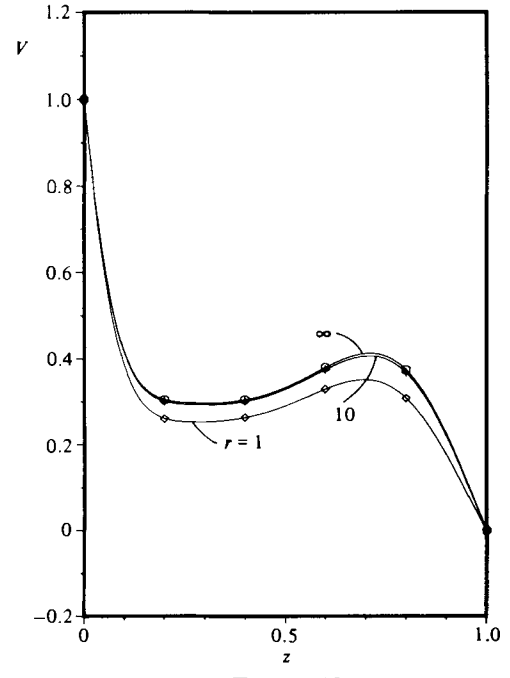

FIGURE 18

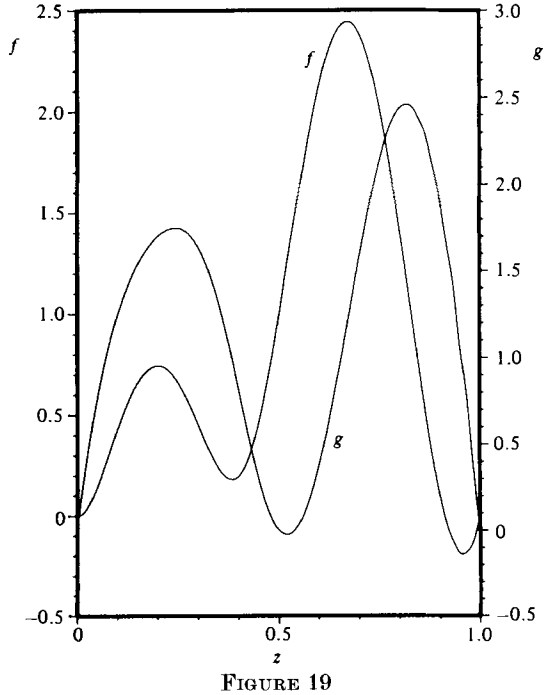

FIGURE 19

FIGURE 18. Tangential component of non-dimensional velocity $V = v/x^1\Omega$; branch I at $E = \frac{1}{275}$, $s = 0$, $\kappa = 0$, $C = 1$, $\theta = \frac{1}{4}\pi$.

FIGURE 19. Branch I at $E = \frac{1}{275}$, $s = -0.25$, $\kappa = 0$, $C = 1$.

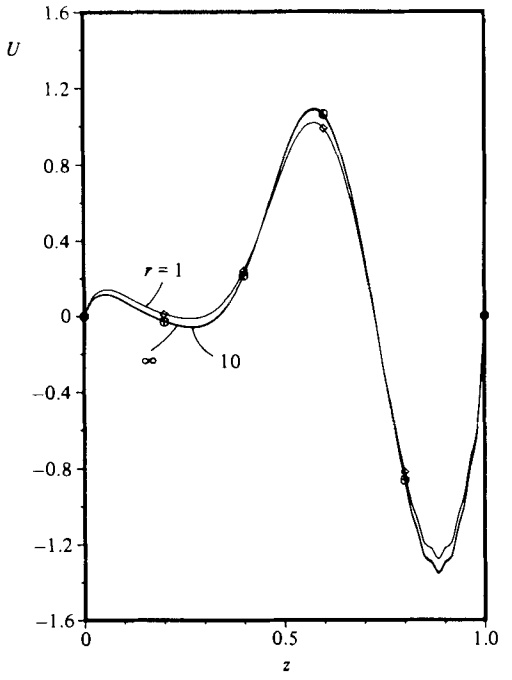

FIGURE 20

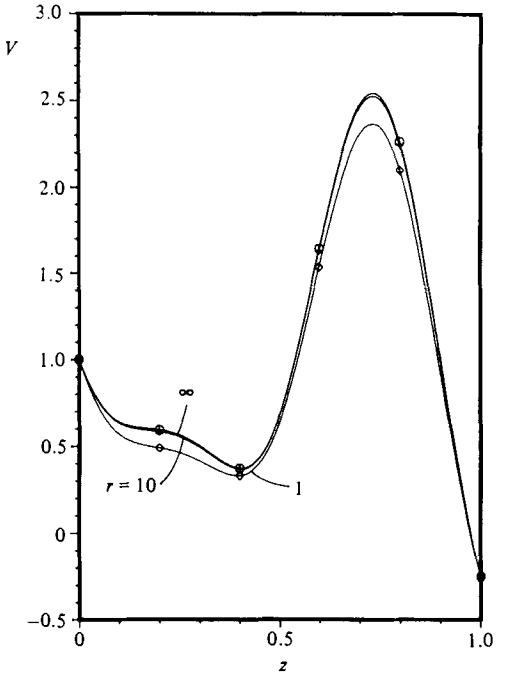

FIGURE 21

FIGURE 20. Radial component of non-dimensional velocity $U = u/x^1\Omega$; branch I at $E = \frac{1}{275}$, $s = -0.25$, $\kappa = 0$, $C = 1$, $\theta = \frac{1}{4}\pi$.

FIGURE 21. Tangential component of non-dimensional veocity $V = v/x^1\Omega$; branch I at $E = \frac{1}{275}$, $s = -0.25$, $\kappa = 0$, $C = 1$, $\theta = \frac{1}{4}\pi$.

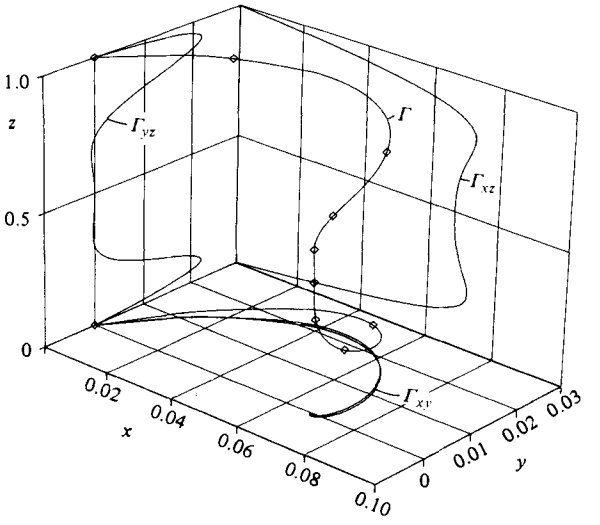

FIGURE 22. Locus of stagnation point; branch I at $E = \frac{1}{275}$, $s = 0.8$, $C = 1$, $\kappa = 0$ ($\Gamma \equiv$ locus; $\Gamma_{xy} \equiv$ projection onto (xy)-plane).

to use a step size $\Delta s = 0.05$ in order to reach convergence of the Newton procedure in not more than 30 iterations ($N = 63$). For $s < 0$ the step size had to be decreased: to reach $s = -0.18$ from $s = 0$ we required 18 steps, or $\Delta s = 0.01$, for convergence within 70 iterations, and a total of 65 minutes CPU time on the PDP-10. We report here on the solution at $s = -0.25$.

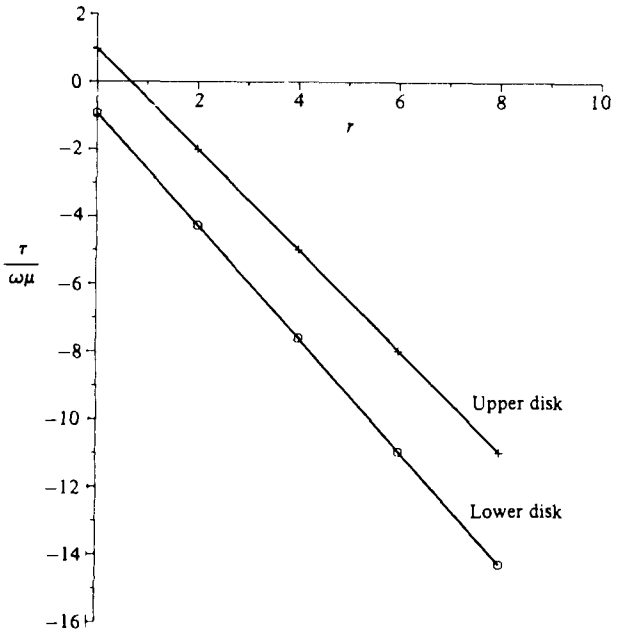

FIGURE 23. Variation of wall stress with radial position; branch I at $E = \frac{1}{275}$, $s = 0.8$, $\kappa = 0$, $\theta = \frac{1}{4}\pi$.

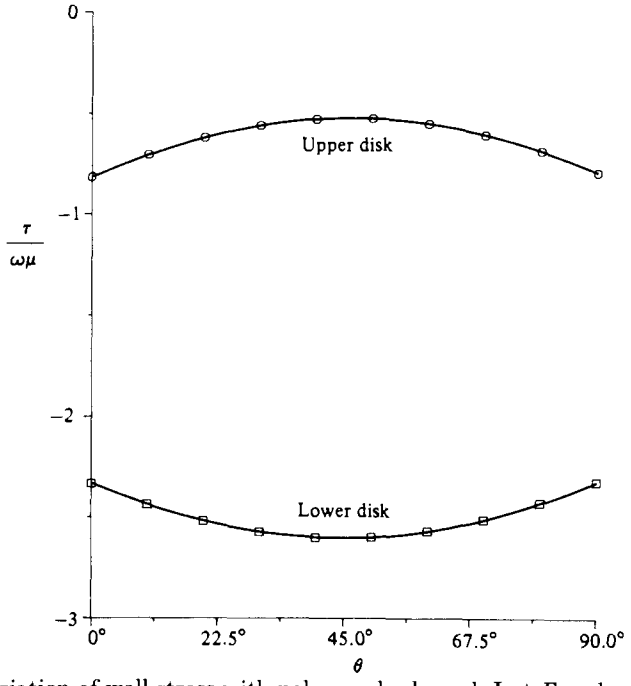

FIGURE 24. Variation of wall stress with polar angle; branch I at $E = \frac{1}{275}$, $s = 0.8$, $\kappa = 0$, $r = 1$.

Figures 19–21 display the branch I solution at $E = \frac{1}{275}$ and $s = -0.25$ (counter-rotating disks). This solution was again obtained from the corresponding solution at $s = 0.8$ by continuation in s. Figure 19 contains $f(z)$ and $g(z)$, $C = 1$. Figures 20 and 21 show radial and tangential components respectively of the non-dimensional velocity at $\theta = \frac{1}{4}\pi$ and various r-positions.

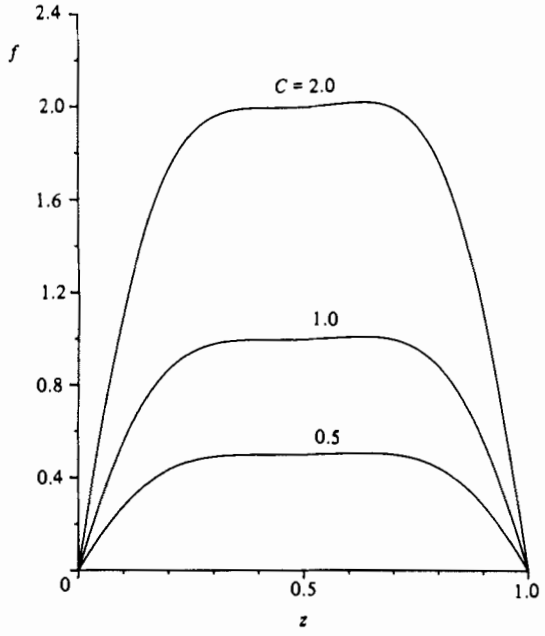

FIGURE 25

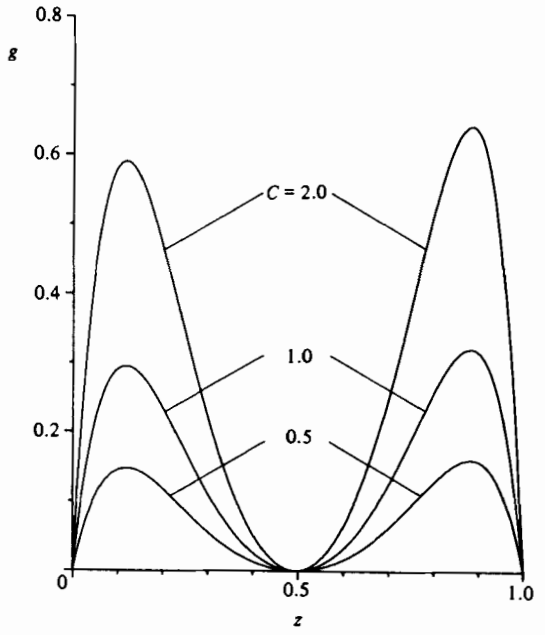

FIGURE 26

FIGURE 25. Effect of constant C; branch I at $E = \frac{1}{100}$, $s = 0.8$, $\kappa = 0$.
FIGURE 26. Effect of constant C; branch I at $E = \frac{1}{100}$, $s = 0.8$, $\kappa = 0$.

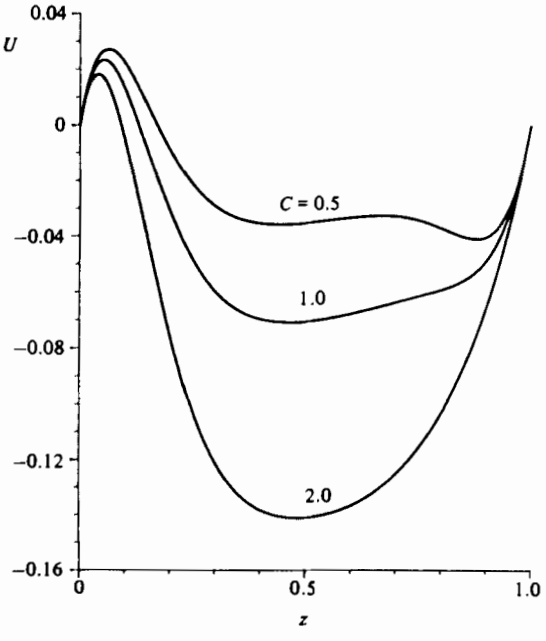

FIGURE 27

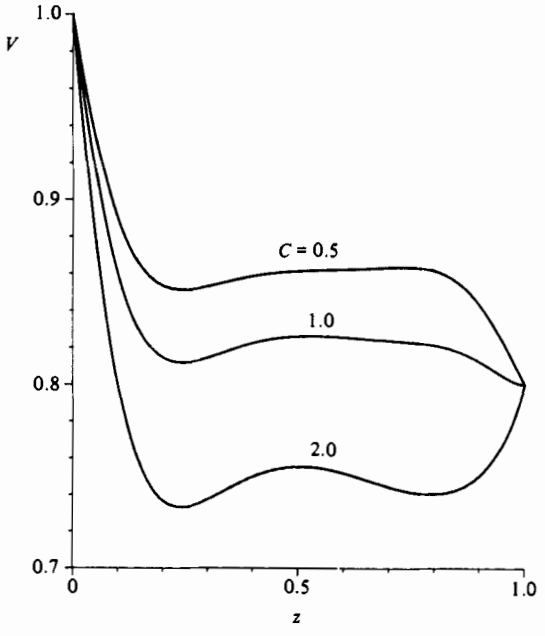

FIGURE 28

FIGURE 27. Effect of constant C; branch I at $E = \frac{1}{100}$, $s = 0.8$, $\kappa = 0$, $r = 1.0$, $\theta = \frac{1}{4}\pi$.
FIGURE 28. Effect of constant C; branch I at $E = \frac{1}{100}$, $s = 0.8$, $\kappa = 0$, $r = 1.0$, $\theta = \frac{1}{4}\pi$.

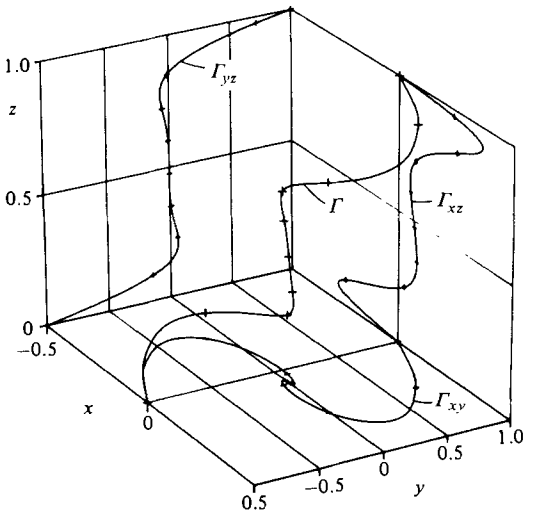

FIGURE 29. Locus of stagnation points; branch I at $E = \frac{1}{275}$, $s = 0.8$, $C = 1$, $\kappa = 1$ ($\Gamma \equiv$ locus; $\Gamma_{xy} \equiv$ projection onto (x, y)-plane).

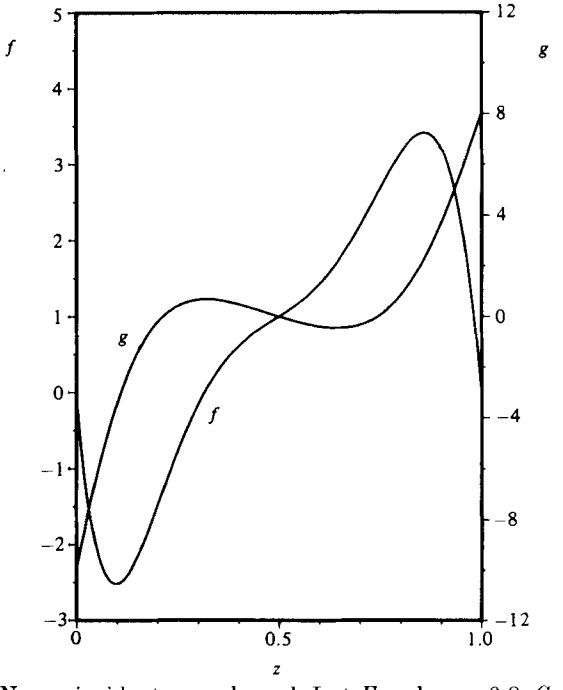

FIGURE 30. Non-coincident axes; branch I at $E = \frac{1}{100}$, $s = 0.8$, $C = 1$, $\kappa = 1$.

Figure 22 is a composite diagram obtained for branch I at $E = \frac{1}{275}$, $s = 0.8$. It contains the locus Γ of the stagnation points ($u = v = 0$) and its projections Γ_{xy}, Γ_{xz} and Γ_{yz}.

We define the non-dimensional wall stress $\bar{\tau}_w$ by normalizing its dimensional counterpart with $\mu\omega$. $\bar{\tau}_w$ is given by

$$\bar{\tau}_w = rG'(z) - E^{\frac{1}{2}}[g'(z)\sin\theta + f'(z)\cos\theta]. \tag{23}$$

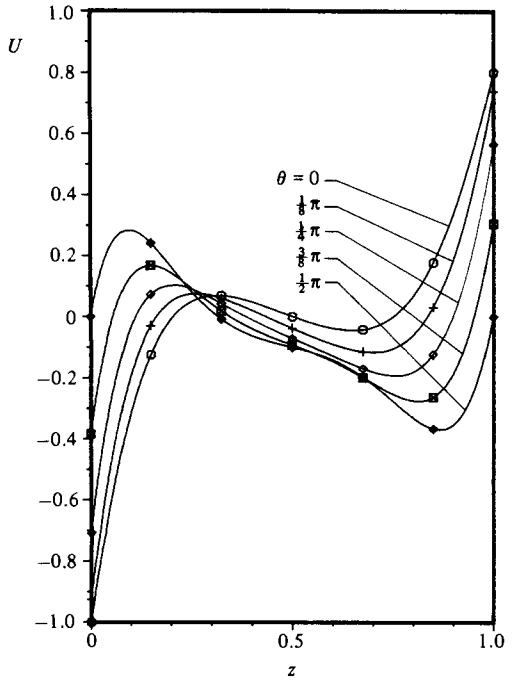

FIGURE 31

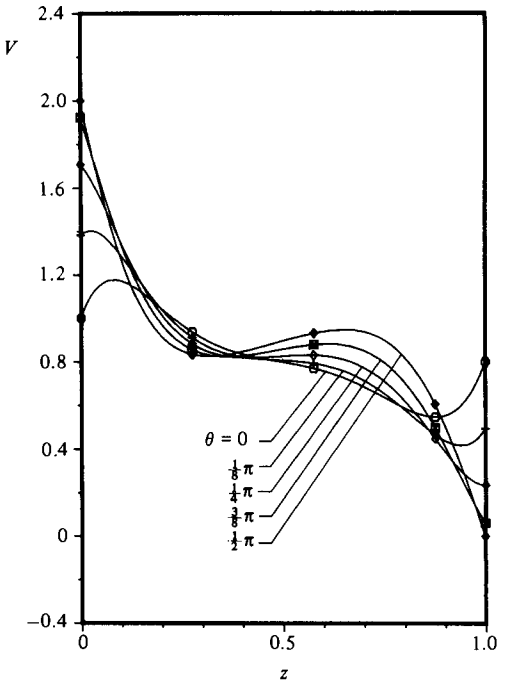

FIGURE 32

FIGURE 31. Development of radial velocity $U = u/x^1\Omega$; non-coincident axes; branch I at $E = \frac{1}{100}$, $s = 0.8$, $C = 1$, $\kappa = 1$, $r = 1$.

FIGURE 32. Development of tangential velocity $V = v/x^1\Omega$; non-coincident axes; branch I at $E = \frac{1}{100}$, $s = 0.8$, $C = 1$, $\kappa = 1$, $r = 1$.

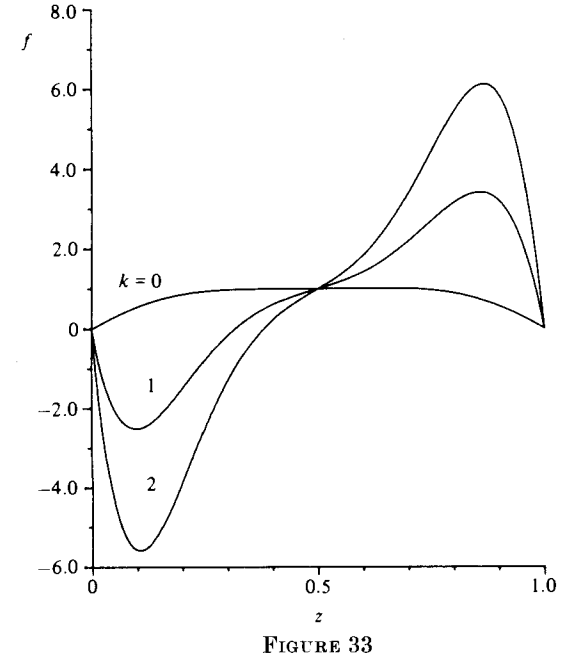

FIGURE 33

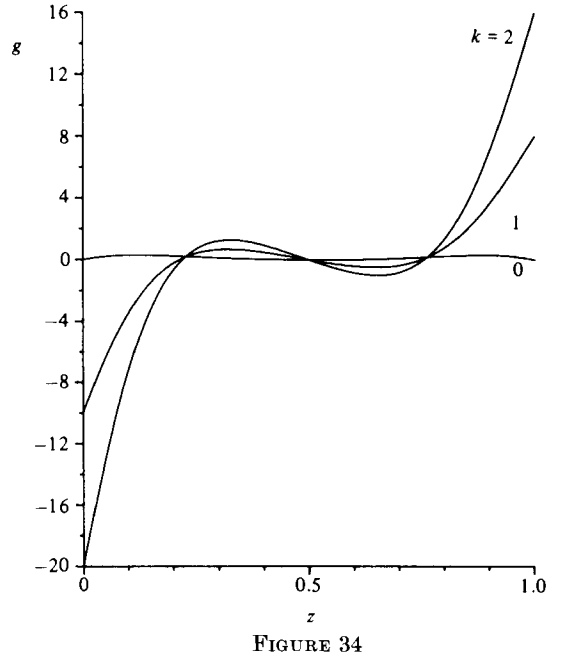

FIGURE 34

FIGURE 33. Effect of distance between non-coincident axes; branch I at $E = \frac{1}{100}$, $s = 0.8$, $C = 1$.

FIGURE 34. Effect of distance between non-coincident axes; branch I at $E = \frac{1}{100}$, $s = 0.8$, $C = 1$.

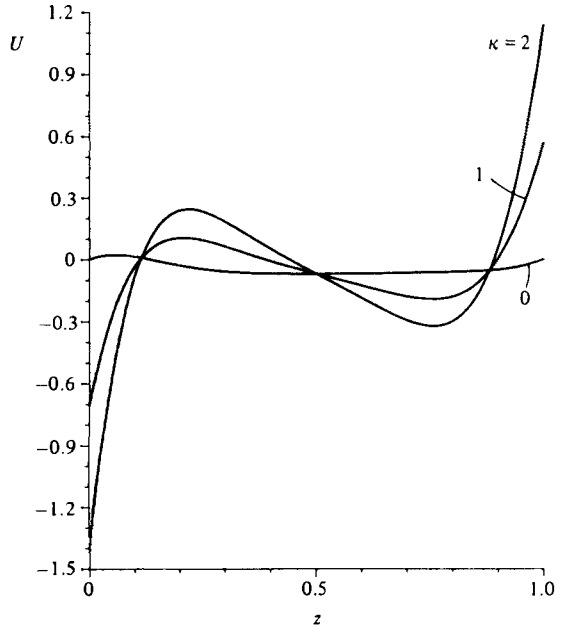

FIGURE 35

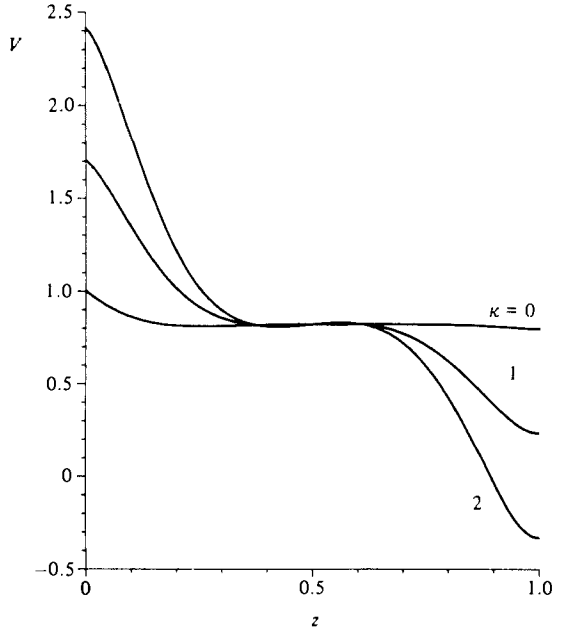

FIGURE 36

FIGURE 35. Effect of distance between non-coincident axes; branch I at $E = \frac{1}{100}$, $s = 0.8$, $C = 1$, $r = 1.0$, $\theta = \frac{1}{4}\pi$.

FIGURE 36. Effect of distance between non-coincident axes; branch I at $E = \frac{1}{100}$, $s = 0.8$, $C = 1$, $r = 1.0$, $\theta = \frac{1}{4}\pi$.

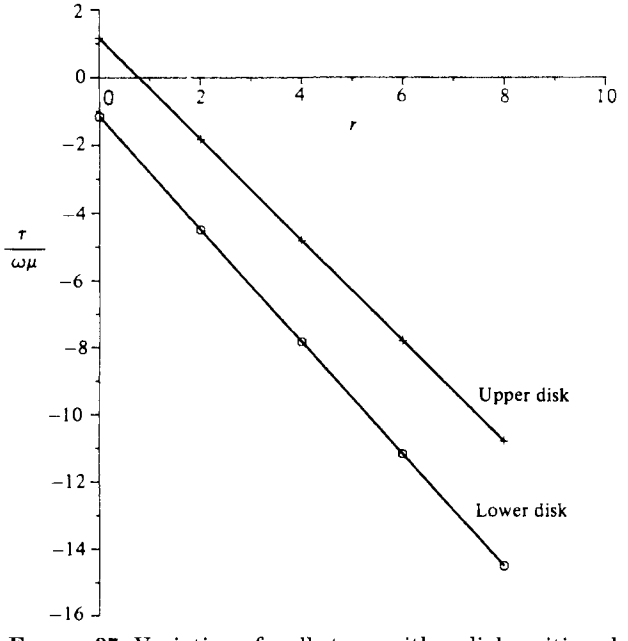

FIGURE 37. Variation of wall stress with radial position; branch I at $E = \frac{1}{275}$, $s = 0.8$, $\kappa = 1$, $\theta = \frac{1}{4}\pi$.

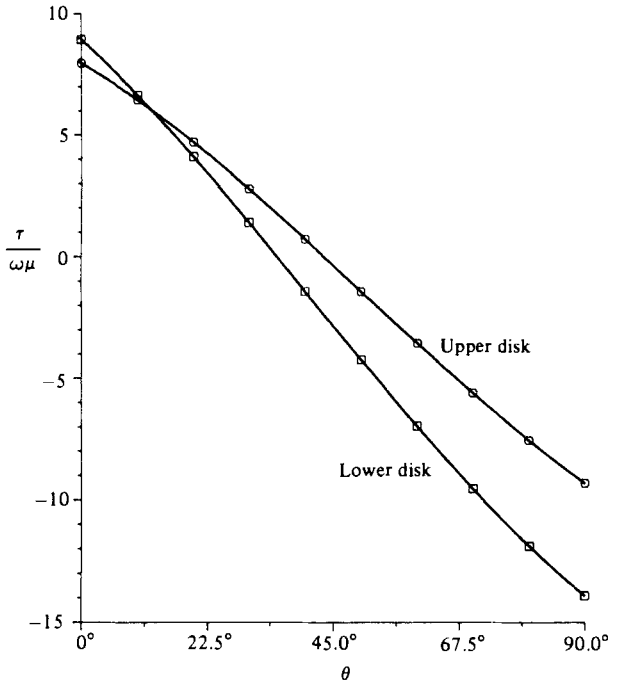

FIGURE 38. Variation of wall stress with polar angle; branch I at $E = \frac{1}{275}$, $s = 0.8$, $\kappa = 1$, $C = 1$, $r = 1.0$.

In figures 23 and 24 we plot $\bar{\tau}_w$ for both upper and lower disks. The wall stress is linear in the distance from the centre of rotation, and there is one value of r for each θ where the wall stress vanishes on the upper disk; for $\theta = \frac{1}{4}\pi$ and $E = \frac{1}{275}$ this value of r is somewhat less than unity. Figure 24 shows the variation of $\bar{\tau}_w$ with azimuthal position at $r = 1$, $E = \frac{1}{275}$.

The constant C in (8) is arbitrary; it specifies the midplane value of the y-component of the translational velocity that (6) superposes on the Kármán solution. Thus C specifies, for a given Kármán flow, the distance between the rotational axis and the stagnation point, for any z = constant plane. Since this relationship between axis and stagnation point is not trivial, it is of interest to study the effect that the value of C has on the flow. Figures 25–28 contain solutions at three distinct values of C, showing that large C enhances the boundary-layer structure of the flow.

4.2. *Non-coincident axes of rotation*

The solutions that we report here were obtained for branch I at $s = 0.8$. The axes of rotation are placed at twice the film thickness apart, and are located in $(\frac{1}{2}, 0, 0)$ for the lower disk and in $(\frac{1}{2}, \pi, 1)$ for the upper disk in the non-dimensional $\{r, \theta, z\}$ coordinate system. Thus $\theta = 0$ in (6) is no longer arbitrary. The locus Γ of stagnation points for axes of rotation separated by twice the film thickness is shown in figure 29 for $E = \frac{1}{275}$. Figure 30 shows the functions $f(z)$ and $g(z)$ at $E = \frac{1}{100}$. To see the effect of non-coincidence of axes, figure 30 is to be compared with figure 2, which was obtained at $\kappa = 0$ and the same value of the Ekman number. Both $f(z)$ and $g(z)$ are almost antisymmetric with respect to the $z = \frac{1}{2}$ plane. They are superposed on $F(z)$ and $G(z)$ to yield the non-dimensional velocity of figures 31 and 32. Moving along the unit circle $r = 1$ from $\theta = 0$ towards $\theta = \frac{1}{2}\pi$, the velocity of the core seems to change

little. What change there is is concentrated in the boundary layers. The principal effect of $f(z)$ and $g(z)$ is to change the wall stress. Figures 33 and 34 depict the variations of $f(z)$ and $g(z)$ respectively with the offset κ for fixed values of E and C. The variations of the velocities U and V, with the offset κ, are given in figures 35 and 36. Finally, in figures 37 and 38, the non-dimensionalized wall shear stresses at the upper and lower disk are plotted as functions of r and θ respectively at $E = \frac{1}{275}$, $\kappa = 1$ and $C = 1$.

5. Summary

We conclude with a few observations on the implications of the results established and discuss some of the questions that remain unanswered.

On the basis of the work of Parter & Rajagopal (1984), we have exhibited numerically, for the first time, asymmetric solutions for the flow between infinite parallel plates, rotating about a common axis or about distinct axes. The existence of such solutions is clearly due to the fact that the plates are assumed to be infinite in extent. Interestingly, these asymmetric solutions are not a feature of high-Reynolds-number flow but are present even at low Reynolds numbers. The stability of these asymmetric solutions warrants close scrutiny. Contrary to intuitive expectation, the analysis of Berker (1979) for his special class of flows answer the question of stability in the affirmative. The stability of the flows exhibited in this paper to infinitesimal disturbances is being carried out. The flow and the stability for the single-disk problem is also being studied in detail.

REFERENCES

Abbot, T. N. & Walters, K. 1970 Rheometrical flow systems. Part 2. Theory of the orthogonal rheometer, including an exact solution of the Navier–Stokes equations. *J. Fluid Mech.* **40**, 205–213.

Adams, M. L. & Szeri, A. Z. 1982 Incompressible flow between finite disks. *Trans. ASME* E: *J. Appl. Mech.* **49**, 1–14.

Batchelor, G. K. 1951 Note on a class of solutions of the Navier–Stokes equations representing rotationally symmetric flow. *Q. J. Appl. Maths* **4**, 29–41.

Berker, R. 1936 *Sur Quelques cas d'Intégration des Equations du Mouvement d'un Fluide Visqueux Incompressible.* Lille, Paris.

Berker, R. 1979 A new solution of the Navier–Stokes equation for the motion of a fluid contained between two parallel planes rotating about the same axis. *Arch. Mech. Stosowanej* **31**, 265–280.

de Boor, C. 1978 *A Practical Guide to Splines.* Springer.

Dijkstra, D. & van Heijst, G. J. F. 1983 The flow between finite rotating disks enclosed by a cylinder. *J. Fluid Mech.* **128**, 123–154.

Greenspan, D. 1972 Numerical studies of flow between rotating coaxial disks. *J. Inst. Maths Applics* **9**, 370–377.

Holodniok, M., Kubíček, M. & Hlaváček, V. 1977 Computation of the flow between two rotating coaxial disks. *J. Fluid Mech.* **81**, 680–699.

Holodniok, M., Kubíček, M. & Hlaváček, V. 1981 Computation of the flow between two rotating coaxial disks: multiplicity of steady-state solutions. *J. Fluid Mech.* **108**, 227–240.

Kármán, T. von 1921 Über laminare und turbulente Reibung. *Z. angew. Math. Mech.* **1**, 233.

Keller, H. B. & Szeto, R. K.-H. 1983 Calculation of flows between rotating disks. Unpublished.

Lance, G. N. & Rogers, M. H. 1961 The axially symmetric flow of viscous fluid between two infinite rotating disks. *Proc. R. Soc. Lond.* A **266**, 109–121.

Mellor, G. L., Chapple, P. J. & Stokes, V. K. 1968 On the flow between a rotating and a stationary disk. *J. Fluid Mech.* **31**, 95–112.

NGUYEN, N. D., RIBAULT, J. P. & FLORENT, P. 1975 Multiple solutions for flow between coaxial disks. *J. Fluid Mech.* **68**, 369–388.

PARTER, S. V. 1982 On the swirling flow between coaxial disks: A survey. In *Theory and Applications of Singular Perturbations*. Lecture Notes in Mathematics, vol. 942. Springer.

PARTER, S. V. & RAJAGOPAL, K. R. 1984 Swirling flow between rotating plates. *Arch. Rat. Mech. Anal.* (in press).

PEARSON, C. E. 1965 Numerical solutions for the time-dependent viscous flow between two rotating coaxial disks. *J. Fluid Mech.* **21**, 623–633.

RAJAGOPAL, K. R. 1981 Flow of a second order fluid between rotating parallel plates. *J. Non-Newt. Fluid Mech.* **9**, 185–190.

RAJAGOPAL, K. R. 1982 On the flow of a simple fluid in an orthogonal rheometer. *Arch. Rat. Mech. Anal.* **79**, 29–47.

RAJAGOPAL, K. R. 1984 A class of exact solutions to the Navier–Stokes equations. *Intl J. Engng Sci.* **22**, 451–458.

RAJAGOPAL, K. R. & GUPTA, A. S. 1981 Flow and stability of a second grade fluid between two rotating parallel plates. *Arch. Mech. Stosowanej* **33**, 663–674.

ROBERTS, S. M. & SHIPMAN, J. S. 1976 Computation of the flow between a rotating and a stationary disk. *J. Fluid Mech.* **73**, 53–63.

SZERI, A. Z. & GIRON, A. 1984 Stability of flow over an infinite rotating disk. *Numer. Meth. Fluids* (in press).

SZERI, A. Z., GIRON, A., SCHNEIDER, S. J. & KAUFMAN, H. N. 1983*a* Flow between rotating disks. Part 2. Stability. *J. Fluid Mech.* **134**, 133–154.

SZERI, A. Z., SCHNEIDER, S. J., LABBE, F. & KAUFMAN, H. N. 1983*b* Flow between rotating disks. Part 1. Basic flow. *J. Fluid Mech.* **134**, 103–131.

WILSON, L. O. & SCHRYER, N. L. 1978 Flow between a stationary and a rotating disk with suction. *J. Fluid Mech.* **85**, 579–496.